

Following Paths of Maximum Catalytic Activity in the Composition Space of High-Entropy Alloys

Mads K. Plenge, Jack K. Pedersen, Vladislav A. Mints, Matthias Arenz, and Jan Rossmeisl*

The search for better and cheaper electrocatalysts is vital in the global transition to renewable energy resources. High-entropy alloys (HEAs) provide a near-infinite number of different alloys with approximately continuous properties such as catalytic activity. In this work, the catalytic activity for the electrochemical oxygen reduction reaction as a function of molar composition of Ag-Ir-Pd-Pt-Ru HEA is treated as a landscape wherein it is shown that the maxima are connected through ridges. By following the ridges, it is possible to navigate between the maxima using a modified nudged elastic band (NEB) model integrated in a machine learning NEB algorithm. These results provide a new understanding of the composition space being similar to an evolutionary landscape. This provides a possible new search and design strategy for new catalysts in which the composition of known catalysts can be optimized by following ridges rather than exploring the whole alloy composition space.

there is theoretically room for improvement.^[4] Finding a cheaper and better catalyst for ORR is therefore vital.^[5,7]

In this search for better catalysts, high-entropy alloys (HEAs) have shown great promise, because they offer an unbounded number of different alloys within a continuous composition space.^[8,9] Because each material will give many different adsorption sites, HEAs can serve as a discovery platform for new catalysts,^[10] with several discoveries recently made using computational models for various catalyzed reactions.^[10–15] The idea of thinking of the catalytic activity as a continuous function of the HEA composition to be optimized in an experimental context where the number of experiments must be kept as

low as possible has developed recently.^[16–19] It was found with simulations that the function of ORR catalytic activity for the Ag-Ir-Pd-Pt-Ru HEA composition space has a relatively long length scale of around 0.3 with respect to molar composition.^[16] This means that the correlation between molar compositions is still expected to be significant even when they are spaced 30 atomic percent (at%) apart in composition space. This matches well experimental investigations of thin-film libraries with continuous variations in the compositions of the same five elements, where the observed length scale comes out the same as in the simulations.^[20]

It is a further investigation of this composition space and its nature that is scrutinized in the current work. We hypothesize that locally optimal catalysts are connected by ridges of suboptimal compositions on the function of catalytic activity. This is analogous to a mountain landscape, where the best catalysts are the mountain tops, and the mountains are connected via ridges. In other words, it is possible that there is a common thread that connects optimal compositions and hence can lead to active catalysts in the composition space. This could be a way to limit where to look in the vast composition space of HEAs. Instead of finding the needle in the haystack, we may only need to find a thread and follow it. Searching for optimal catalysts by following ridges is analogous to mutations in a biological evolutionary fitness landscape, where small gradual mutations following the ridge will lead to an increase in fitness while going too far off the path of the ridge may lead to extinction.^[21] Thus, the composition space can be treated like an evolutionary landscape where the mutations are slight changes in molar fractions of elements.


In the current work, simulations of the electrochemical ORR are used to model the landscape of the catalytic activity as a function of the composition of the quinary Ag-Ir-Pd-Pt-Ru alloy.

1. Introduction

The globe faces a grand challenge with increasing energy demand and global warming accelerated by greenhouse gases. An important part of transitioning to renewable energy sources is efficient energy conversion and storage.^[1–3] Converting energy from renewable energy into chemical fuels, which, e.g., is possible via water splitting, will play an important part in the transition from fossil fuels.^[1,4] A way to extract the energy is by the use of hydrogen fuel cells, where oxygen and hydrogen recombine to form water where the oxygen reduction reaction (ORR) plays a major role.^[4,5] This reaction must be catalyzed, but today's most used catalyst is platinum which is scarce and expensive,^[1,5–7] and

M. K. Plenge, J. K. Pedersen, M. Arenz, J. Rossmeisl
Center for High Entropy Alloy Catalysis (CHEAC)
Department of Chemistry
University of Copenhagen
Universitetsparken 5, 2100 København Ø, Denmark
E-mail: jan.rossmeisl@chem.ku.dk

V. A. Mints, M. Arenz
Department for Chemistry
Biochemistry and Pharmaceutical Sciences
University of Bern
Freiestrasse 3, 3012 Bern, Switzerland

 The ORCID identification number(s) for the author(s) of this article can be found under <https://doi.org/10.1002/aenm.202202962>.

© 2022 The Authors. Advanced Energy Materials published by Wiley-VCH GmbH. This is an open access article under the terms of the Creative Commons Attribution License, which permits use, distribution and reproduction in any medium, provided the original work is properly cited.

DOI: 10.1002/aenm.202202962

Being composed of noble metals, this HEA is expected to show superior corrosion resistance and therefore is a candidate that would make for easier comparison with experimental tests. The HEA is, however, at best expected to be meta-stable with surface segregation and surface dissolution being inevitable for prolonged experimental durations. Prediction of the meta-stability of the alloy surfaces has not been carried out in the current study as it is out of the scope of the presented analysis since even transitory surface compositions can be associated with a catalytic activity. However, meta-stability remains an interesting path of investigation for the field of HEA catalysis. Simulation of the catalytic activity is achieved by applying a previously applied^[16] kinetic model for each individual catalyst surface site, considering a face-centered cubic (fcc) (111) disordered surface of the HEA. Trained on hundreds of density functional theory (DFT) simulations, the model estimates adsorption energies of *OH and *O and outputs a measure of catalytic activity, the current density, based on these. The adsorption energies of *OH and *O have been simulated relative to those of Pt(111) which has been found to bind *OH and *O about 0.1 and 0.2 eV too strongly compared to the optimal adsorption energy through tight collaboration between simulations and experiments.^[22] In this way the adsorption energies of *OH and *O emerge as the most important descriptors for ORR catalytic activity on comparable alloy surfaces and many interface effects, such as adsorbate solvation can be eliminated in this comparison (see Section S1, Supporting Information). The model has previously been shown to have satisfactory predictive power in experiments on the Ag-Ir-Pd-Pt-Ru composition space,^[20] with multiple locally optimal compositions detected.^[16] It is found that maxima of catalytic activity in composition space are indeed connected through ridges in this landscape and a new strategy for searching for catalysts is suggested in which already optimal catalyst in one composition space are optimized even further in another.

2. Results and Discussion

2.1. Connecting Maxima via Ridges

The concept of connecting points via ridges has been especially useful in the search for minimum energy pathways for chemical reactions where the coordinates are expressed in terms of atomic configurations. One way to obtain the minimum energy pathway is with the nudged elastic band (NEB) algorithm^[23,24] and its machine learning variants.^[25,26] In the current work, a revised NEB algorithm was implemented to connect two compositions via ridges on the function for catalytic activity obtained with the kinetic model described above (see Section S2, Supporting Information).

The implemented NEB algorithm works by creating an elastic band which is fastened at two end points, here two compositions. The band itself is defined by a set of points, traditionally called images, corresponding to a molar composition with springs between each image giving rise to the elasticity. The elastic band is nudged orthogonally to the gradients of the catalytic activity function to make it follow the ridges. These ridges thus correspond to the maximum activity pathways.

The activity function which the NEB operates on, and which forms the activity landscape, is modelled using a Gaussian process regressor (GPR) fitted to simulations of the catalytic ORR activity (see Section S3, Supporting Information). The compositions for these simulations were sampled on a uniform grid with a spacing of 5 at% of the Ag-Ir-Pd-Pt-Ru composition space. The GPR activity function has a 2% mean relative prediction error and a coefficient of determination (R^2 value) of 0.996 compared to the results obtained with simulations (see Figure S3, Supporting Information). It has an absolute error of ≈ 0.001 (arb. units), which is on the same order of magnitude as the standard deviation of the kinetic model.^[16] By using the GPR activity function for the NEB algorithm rapid evaluations of the activity are enabled, while at the same time maintaining the same accuracy as if simulations from the model were called in series. The continuity and differentiability possessed by the smooth GPR activity function is reasonable to assume for the real activity function that would be produced in an experimental realization as well as the currently employed kinetic model. The reason is that a smoothly varying activity functions has previously been observed for the current HEA.^[20]

All pure metals were connected in each of the 10 ternary subspaces of Ag-Ir-Pd-Pt-Ru (see Figure S4, Supporting Information), demonstrating that the NEB algorithm forms a path along a ridge, given there is any, between the chosen end points. If one combines these ternary composition spaces along their edges, it becomes apparent that the ridges connect when going to a different ternary composition space. **Figure 1** is a result of this idea. Here, a known active binary catalyst,^[16] namely Ir₄₅Pt₅₅, in the data is chosen as a starting point. The third element to describe the initial ternary composition space is picked arbitrarily as Pd and it is chosen as the final point in the NEB algorithm. When the NEB algorithm has converged, it identifies the maximum point on an opposite edge from the initial edge. Then, the element which is no longer in the composition gets substituted with a random new element that was not in the previous composition, thereby changing the composition space. Figure 1 shows the seven first ternary subspaces that the algorithm went through, stitched together. The nonconnected red

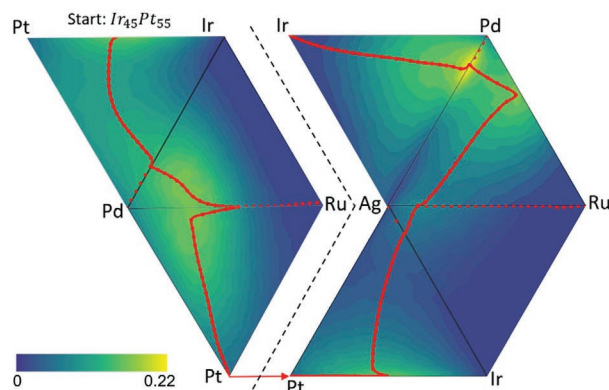


Figure 1. Substituting elements through ternary subspaces starting at Ir₄₅Pd₅₅. The red dots are images, and the solid red line is an interpolated path between the images. The contour plot shows the value of the catalytic activity function in arbitrary units from the regular 5 at% grid of simulations with the kinetic model.

dots are the images going from the maximum edge image to the final image.

The simulation successfully manages to walk along the ridges through compositions to find the global maximum $\text{Ag}_{17}\text{Pd}_{83}$. Along this path it passes through all local maxima within the ternary compositions in the data, which we have found previously.^[16] From this it thus seems that all maxima are indeed connected through ridges, at least in the ternary composition spaces. It also suggests the substitution of elements at edges as a possible new search strategy for optimizing already active catalysts even further.

Since the maxima are connected by ridges in the ternary composition spaces, it was investigated whether this also holds in higher dimensions. This hypothesis was tested by connecting two pure metals through the entire quinary composition space of Ag-Ir-Pd-Pt-Ru by doing multiple climbing images, which are images accelerated directly along the gradient (see Section S2, Supporting Information). With Ag as the initial image and Ir as the final image, it is seen in **Figure 2a** that the path does indeed go through several maxima. It actually goes through all four noticeable maxima found previously^[16] with Bayesian optimization: $\text{Ag}_{85}\text{Ru}_{15}$, $\text{Ag}_{17}\text{Pd}_{83}$, $\text{Ir}_{10}\text{Pd}_{65}\text{Ru}_{25}$, and $\text{Ir}_{49}\text{Pt}_{51}$.

2.2. Following Ridges by Sampling

The NEB algorithm requires many simulations of the catalytic activity of a given composition which is why it is run on the fitted GPR. However, were this to be used in an experimental application, the algorithm must be able to choose compositions by itself and find the same path without sampling the whole space. The machine learning (ML) NEB method attempts to

solve this challenge by sampling the most uncertain image in each iteration until the path converges (see Section S4, Supporting Information). In **Figure 3**, the converged ML NEB path is compared to the classic NEB path for Ag to Pd in the ternary Ag-Ir-Pd composition space. The found path clearly resembles the classic one with negligible deviation. The ML NEB used only 33 evaluations in this case. In comparison, the 5 at% ternary grid contains 231 samples. All 10 ternary subspaces connecting all metals with comparison to the classic NEB algorithm were equivalently evaluated, showing overall good agreement (see Figure S7, Supporting Information). The average number of samples for each ternary composition space was 50 and a standard deviation of 15 samples. The only way to get better results would be to draw more samples, which could lower the uncertainty. However, it would not ensure a different path found as there is limited exploration as it is constrained to the path. It should also be noted that in some of the cases with discrepancies, the ML NEB algorithm finds a seemingly more satisfactory path compared to the classic NEB algorithm (see, e.g., Ag-Ir-Ru (right column) in Figure S7, Supporting Information). The convergence of the uncertainty of the ML NEB algorithm with the number of samples varies between composition spaces, and in a very few cases the convergence criterion acts as an asymptote (see Figure S8, Supporting Information).

Figure 1 that was made with data from the classic NEB algorithm was recreated using the ML NEB algorithm, and the two show almost identical ridges (see Figure S9, Supporting Information), making this a possible experimental strategy in practice. When starting on the ridge in the ternary composition space, the ML NEB in general converged with less samples than when connecting between pure metals (see Table S1, Supporting Information).

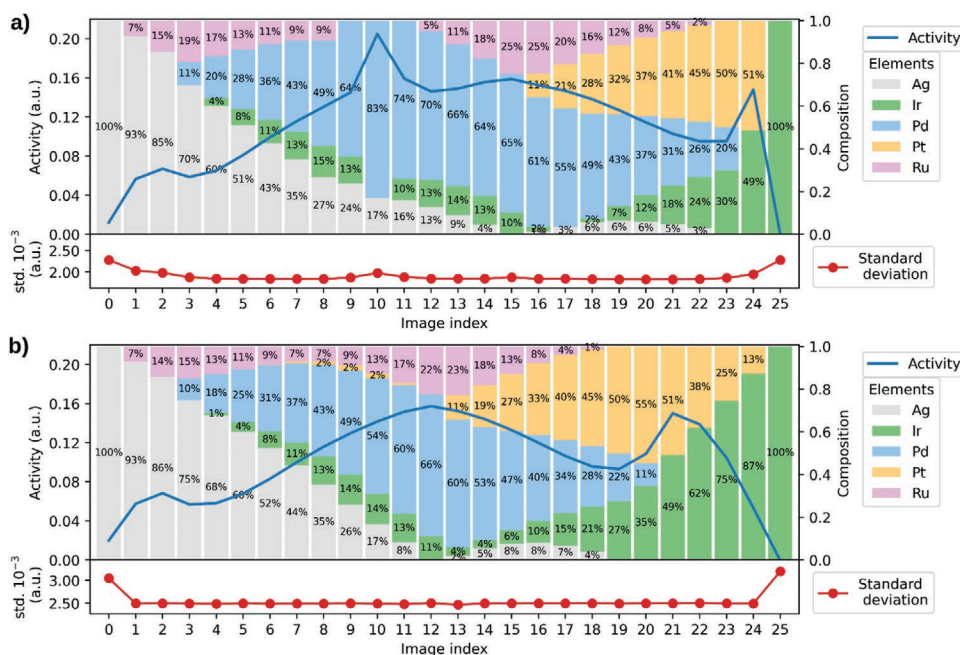


Figure 2. Activity height profile of the converged NEB paths between Ag and Ir for the classic NEB algorithm using the GPR model trained on a uniform 5 at% grid a), and for the ML NEB algorithm with convergence after 269 samples b). In the background the molar fractions are displayed and at the bottom is the uncertainty from the GPR prediction at each point.

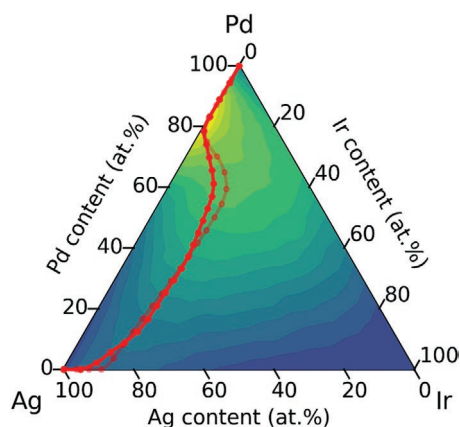


Figure 3. ML NEB compared to classic NEB. The converged ML NEB is shown clear while the path found from the classic NEB is faded. Same color scale for the contour plot as in Figure 1.

For the ML NEB algorithm to be more effective as an experimental strategy it should be scalable in dimensions, i.e., with more elements. From Figure 2a, it seems that the NEB algorithm is able to follow ridges between maxima in the quinary space. Moreover, by connecting Ag and Ir, several maxima, including the global maximum $\text{Ag}_{17}\text{Pd}_{83}$, were found. When using the ML NEB algorithm, nearly the same path through the composition space is found as for the NEB algorithm as shown in Figure 2b. However, the global maximum $\text{Ag}_{17}\text{Pd}_{83}$ is bypassed in this case. One possible explanation for this is that the ML NEB algorithm is missing gradient information to point it toward the optimal composition $\text{Ag}_{17}\text{Pd}_{83}$.

In general, it seems that for an increasing dimensionality of the composition space, it becomes increasingly more difficult for the GPR, via the ML NEB, to get an accurate prediction of the whole space. The fact that the $\text{Ag}_{17}\text{Pd}_{83}$ maximum is quite narrow in composition space, see for example Figure 3, supports this idea. To find this specific maximum, there must be samples close to it, which is the case when choosing Ag and Pd as initial and final compositions in quinary composition space as well as Ir and Pd (see Figure S10, Supporting Information). The reason is that the maximum is close to one of the end points of the ML NEB.

Traditionally for the ML NEB algorithm for atomic systems, gradient information is used in the GPR to increase the accuracy of the predicted function.^[25,26] However, in the current work the surface is not an energy surface, and the gradient information cannot be directly extracted from the simulations of the catalytic activity. Gradient information in the GPR would likely provide faster and more accurate convergence of the paths. The reason for $\text{Ag}_{17}\text{Pd}_{83}$ being difficult for the ML NEB to find could also in part be due to the shape of the ridge throughout the composition space. It seems like the ridge going toward $\text{Ag}_{17}\text{Pd}_{83}$ from the ridge path in Figure 2a is not a continuation of the ridge but rather a blind alley, since the molar fraction of the images before and after $\text{Ag}_{17}\text{Pd}_{83}$ (image index 9 and 11 in Figure 2a) seem to represent the same path, indicating that the found pathway turns back around at $\text{Ag}_{17}\text{Pd}_{83}$.

In an attempt to understand the nature of the ridges in composition space and especially in higher dimensions where it

cannot be plotted, a ridge detection algorithm was developed, which can determine if a given point is on a d -dimensional ridge directly from the trained GPR (see Section S5, Supporting Information). The ridge detection algorithm does confirm that the NEB indeed follows ridges, also in higher dimensions (see Figures S11–S14, Supporting Information). However, the ridge detection algorithm revealed potential problems with the GPR in the composition space. The reason is that ridges would be detected at unexpected locations, where in some cases this could be attributed to the way the GPR has learned the landscape of catalytic activity. This includes forming maxima of catalytic activity outside the simplex that is bounding the composition space (see Figure S15, Supporting Information). This is especially a problem for the shape of the 1D-ridges, i.e., one-dimensional curves that are maximized with respect to all directions that are orthogonal to the direction of the ridge itself, which are the ones of interest in higher dimensional composition spaces. The unphysical maxima that the GPR learns influence the shape of the 1D-ridges, making the combination of the GPR and ridge detection unsuitable to get a reliable trace of the ridges in higher dimensional composition space.

From the results using the NEB algorithm it is indeed possible to follow ridges between maxima on the activity function in composition space. The exact shape and interconnectivity of these ridges in higher dimensions is still not perfectly understood and the GPR shows some limitations because it is bounded by a hyperdimensional simplex in composition space. It is also not entirely conclusive whether all local maxima are connected via ridges in higher dimensions. The fact that the classic NEB algorithm in the quinary composition space seems able to connect most maxima, without the height profile of the activity dropping to zero or near-zero between maxima (see, e.g., Figure 2a), indicates that the maxima are indeed still connected via ridges in higher dimensional space.

To further investigate the nature of this activity landscape and the behavior of the model in general by studying an arbitrary activity function, randomly generated parameters for the kinetic model, corresponding to “artificial elements,” were chosen to model a different activity function (see Section S6, Supporting Information). Even though the activities were much smaller with the generated artificial elements, the activity landscape was still showing ridges and it was possible to navigate between the maxima using the element substitution strategy with ML NEB (see Figure S16, Supporting Information).

2.3. Directed Evolution to Follow Ridges

A downside of using a NEB algorithm is that the found path depends on the initial and final composition. To circumvent this and to further explore the analogy of the evolutionary landscape, a possible experimental strategy similar to directed evolution^[27] (DE) is suggested (see Section S7, Supporting Information). Figure 4 shows the results of a DE simulation through ternary compositions. The DE was started at a composition, $\text{Ir}_{50}\text{Pt}_{50}$, with a relatively good activity to show how an already well-performing catalyst can be optimized further. The DE then progressed through several maxima by following the ridge. Interestingly the path seems to get “trapped” around

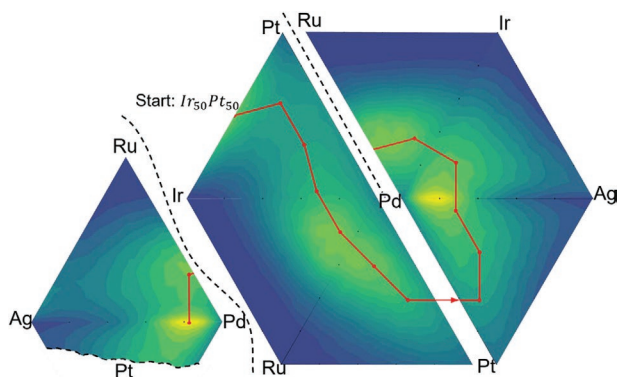


Figure 4. Simulation of DE starting at $\text{Ir}_{50}\text{Pt}_{50}$ in the Ir-Pd-Pt composition space. The path taken through six ternary composition spaces plus the final selected mutation is shown. In this simulation the maximum mutation angle was set to 90° , i.e., the path was allowed to make turns of maximally 90° . This would limit the tendency to go back to an already discovered maximum. The number of mutations made in each step was 13. The activities of the mutations are simulated with the kinetic model. The path is plotted on contour plots based on the 5 at% grid data.

palladium, circling around it along the ridge. Ridges around Pd is also visible in Figure S12 (Supporting Information). The selected points do not sample the exact maxima and are unlikely to do so, because of the relatively big and constant step length of 25 at% that was found to be appropriate for these simulations. To sample the maxima between the sampled points on the path, one could for example use Bayesian optimization in one dimension along the path or just simple intuition to predict where the maximum may lie. In Figure 4, the simulations on ternary composition spaces only are shown to visualize the concept in the activity landscape, but the strategy is scalable in dimensions.

As presented in this work, the evolutionary landscape only has one fitness parameter, namely the catalytic activity. Other fitness parameters to influence the landscape could be stability or simply the cost of the materials. To get an idea of how the scarcity of the constituent elements could influence the fitness landscape, the catalytic activity is plotted against a measure of the scarcity, the inverse of the production rates of the constituent elements normalized to the production rate of Pt, for all compositions on a uniform 5 at% grid of the Ag-Ir-Pd-Pt-Ru HEA composition space. The results are shown in Figure 5. The Pareto optima^[28] are the points at which improving either the catalytic activity or alleviating the element scarcity necessarily leads to worsening of the other. Because Ag is produced in markedly larger proportions than the remaining elements, most of the Pareto front, i.e., the set of Pareto optima, essentially comes out as Ag-Pd binary alloys in various proportions.

By introducing the scarcity of the constituent elements, the interesting compositions are no longer just the ones with the highest catalytic activity, but also those that are composed of abundant elements. Had the element scarcity been introduced as a fitness parameter in the DE simulation, the path taken would likely have favored the Pareto optimal compositions. Thus, favoring compositions that have high concentrations of Ag.

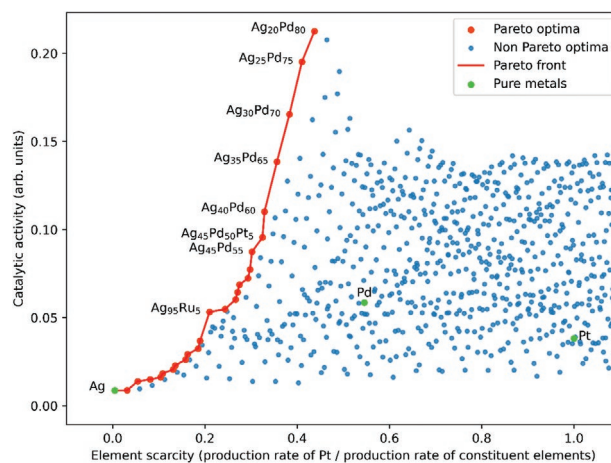


Figure 5. Pareto optima found from a 5 at% grid of all compositions of Ag-Ir-Pd-Pt-Ru. The Pareto efficient points are shown in red, the Pareto inefficient in blue. The shown plot is an excerpt of a full range plot (see Figure S17, Supporting Information). Production rates of the elements are obtained from ref. [29].

Overall, the results show that the catalytic activity function indeed behaves comparatively to an evolutionary landscape in composition space. By making small “mutations” in the composition, the activity can be continuously altered. By moving along the ridges, the maxima can be reached. This has the implication that when experimentally looking for a new catalyst, it is a feasible strategy to start from what is known to be a well-performing catalyst and then locating the ridges around it. The element substitution in Figures 1 and 4 are both simulations of this idea. To illustrate the differences between the presented classic NEB, the ML NEM, and the DE algorithms if applied in an experimental realization, two optima, $\text{Ir}_{50}\text{Pt}_{50}$ and $\text{Ag}_{17}\text{Pd}_{83}$ were connected through two ternary composition spaces, Ir-Pd-Pt and Ag-Ir-Pd. The cost of the methods was measured as the number of samples necessary to follow the ridge from one optimum to the other, because both experimentally and computationally with our kinetic model, making and measuring a sample is the time limiting step. The NEB, ML NEB, and DE algorithms were found to need 4717, 112, and 52 samples, respectively (Figure S18 and Table S2, Supporting Information). Thus, while all three algorithms are able to find a connecting ridge between the optima, it shows that the classic NEB approach is not practical when the composition space is not already known.

In terms of finding the global maximum within a larger composition space, Bayesian optimization^[16] with its nonlocal sampling may turn out to be the fastest strategy compared to the locally constrained ML NEB and DE algorithms. A combination with Bayesian optimization could be an even better strategy. Finding ridges could help the Bayesian optimization on to which directions to look and steer it away from uninteresting areas, which likely is the greater part of the vast composition space. The fact that there are ridges within the composition space could be exploited when designing catalyst. If one can design a catalyst so that when it starts decomposing, it will do so along a ridge, it could thereby theoretically lose less catalytic activity over time.

3. Conclusion

By modeling the composition space using a GPR and by modifying the NEB algorithm, paths following ridges of catalytic activity in composition space were produced. Using a developed ridge detection algorithm on the GPR predicted activity function, it was shown that the maxima are indeed connected by ridges in ternary and quaternary compositions. Furthermore, an ML NEB algorithm was implemented, and for the ternary compositions the ML NEB was shown to make accurate predictions of the paths of maximum catalytic activity with relatively few calculations compared to the classic NEB algorithm. In higher dimensions the performance of the ML NEB was less robust in finding the maximum activity path that was found with the classical NEB algorithm.

A possible new strategy of following the ridges of catalytic activity to an edge in composition space followed by substitution of one element with another has been suggested and simulated on ternary compositions. This strategy resembles an evolutionary landscape in which substitution of elements correspond to mutations. By introducing more fitness parameters, the fitness landscape can be altered to find the Pareto efficient compositions in terms of the parameters. Thus, not limiting the search for just the most catalytically active compositions. The evolutionary behavior of the composition space may alter how this vast space is conceived and provides new ways of thinking when both searching for and designing new catalysts.

Supporting Information

Supporting Information is available from the Wiley Online Library or from the author.

Acknowledgements

This work was supported by the Danish National Research Foundation Center for High Entropy Alloy Catalysis (CHEAC) DNRF-149.

Conflict of Interest

The authors declare no conflict of interest.

Data Availability Statement

The data that support the findings of this study are available in the supplementary material of this article.

Keywords

electrocatalysis, high-entropy alloys, oxygen reduction reaction, ridges

Received: August 30, 2022

Revised: October 28, 2022

Published online: November 24, 2022

- [1] S. Chu, Y. Cui, N. Liu, *Nat. Mater.* **2017**, *16*, 16.
- [2] S. P. S. Badwal, S. S. Giddey, C. Munnings, A. I. Bhatt, A. F. Hollenkamp, *Front. Chem.* **2014**, *2*, 79.
- [3] X. Zhang, X. Cheng, Q. Zhang, *J. Energy Chem.* **2016**, *25*, 967.
- [4] A. Kulkarni, S. Siahrostami, A. Patel, J. K. Nørskov, *Chem. Rev.* **2018**, *118*, 2302.
- [5] X. Tian, X. F. Lu, B. Y. Xia, X. W. D. Lou, *Joule* **2020**, *4*, 45.
- [6] M. Shao, Q. Chang, J.-P. Dodelet, R. Chenitz, *Chem. Rev.* **2016**, *116*, 3594.
- [7] H. A. Gasteiger, N. M. Marković, *Science* **2009**, *324*, 48.
- [8] E. P. George, D. Raabe, R. O. Ritchie, *Nat. Rev. Mater.* **2019**, *4*, 515.
- [9] T. Löffler, A. Ludwig, J. Rossmeisl, W. Schuhmann, *Angew. Chem., Int. Ed.* **2021**, *60*, 26894.
- [10] T. A. A. Batchelor, J. K. Pedersen, S. H. Winther, I. E. Castelli, K. W. Jacobsen, J. Rossmeisl, *Joule* **2019**, *3*, 834.
- [11] J. K. Pedersen, T. A. A. Batchelor, A. Bagger, J. Rossmeisl, *ACS Catal.* **2020**, *10*, 2169.
- [12] W. A. Saidi, W. Shadid, G. Veser, *J. Phys. Chem. Lett.* **2021**, *12*, 5185.
- [13] W. A. Saidi, *J. Phys. Chem. Lett.* **2022**, *13*, 1042.
- [14] W. A. Saidi, T. Nandi, T. Yang, *Electrochem. Sci. Adv.* **2022**, <https://doi.org/10.1002/elsa.202100224>.
- [15] X. Wan, Z. Zhang, W. Yu, H. Niu, X. Wang, Y. Guo, *Patterns* **2022**, *3*, 100553.
- [16] J. K. Pedersen, C. M. Clausen, O. A. Krysiak, B. Xiao, T. A. A. Batchelor, T. Löffler, V. A. Mints, L. Banko, M. Arenz, A. Savan, W. Schuhmann, A. Ludwig, J. Rossmeisl, *Angew. Chem., Int. Ed.* **2021**, *60*, 24144.
- [17] A. S. Nugraha, G. Lambard, J. Na, M. S. A. Hossain, T. Asahi, W. Chaikittisilp, Y. Yamauchi, *J. Mater. Chem. A* **2020**, *8*, 13532.
- [18] Y. Zhang, T. C. Peck, G. K. Reddy, D. Banerjee, H. Jia, C. A. Roberts, C. Ling, *ACS Catal.* **2022**, *12*, 10562.
- [19] M. Kim, M. Y. Ha, W.-B. Jung, J. Yoon, E. Shin, I.-d. Kim, W. B. Lee, Y. Kim, H.-t. Jung, *Adv. Mater.* **2022**, *34*, 2108900.
- [20] T. A. A. Batchelor, T. Löffler, B. Xiao, O. A. Krysiak, V. Strotkötter, J. K. Pedersen, C. M. Clausen, A. Savan, Y. Li, W. Schuhmann, J. Rossmeisl, A. Ludwig, *Angew. Chem., Int. Ed.* **2021**, *60*, 6932.
- [21] F. J. Poelwijk, D. J. Kiviet, D. M. Weinreich, S. J. Tans, *Nature* **2007**, *445*, 383.
- [22] I. E. L. Stephens, A. S. Bondarenko, U. Grønberg, J. Rossmeisl, I. Chorkendorff, *Energy Environ. Sci.* **2012**, *30*, 6744.
- [23] G. Henkelman, B. P. Uberuaga, H. Jónsson, *J. Chem. Phys.* **2000**, *113*, 9901.
- [24] D. Sheppard, R. Terrell, G. Henkelman, *J. Chem. Phys.* **2008**, *128*, 134106.
- [25] J. A. Garrido Torres, P. C. Jennings, M. H. Hansen, J. R. Boes, T. Bligaard, *Phys. Rev. Lett.* **2019**, *122*, 156001.
- [26] O.-P. Koistinen, F. B. Dagbjartsdóttir, V. Ásgeirsson, A. Vehtari, H. Jónsson, *Holzforschung* **2017**, *147*, 152720.
- [27] F. H. Arnold, *Angew. Chem., Int. Ed.* **2018**, *57*, 4143.
- [28] M. P. Andersson, T. Bligaard, A. Kustov, K. E. Larsen, J. Greeley, T. Johannessen, C. H. Christensen, J. K. Nørskov, *J. Catal.* **2006**, *239*, 501.
- [29] P. C. K. Vesborg, T. F. Jaramillo, *RSC Adv.* **2012**, *2*, 7933.